

# 3-D boundary element–finite element method for the dynamic analysis of piled buildings \*

L.A. Padrón, J.J. Aznárez, O.Maeso

Instituto Universitario de Sistemas Inteligentes y Aplicaciones Numéricas en Ingeniería  
(SIANI) Universidad de Las Palmas de Gran Canaria  
Edificio Central del Parque Científico y Tecnológico  
Campus Universitario de Tafira, 35017, Las Palmas de Gran Canaria, Spain  
{lpadron,jjaznarez,omaeso}@siani.es

14 September 2010

## Abstract

A boundary element – finite element model is presented for the three-dimensional dynamic analysis of piled buildings in the frequency domain. Piles are modelled as compressible Euler-Bernoulli beams founded on a linear, isotropic, viscoelastic, zoned-homogeneous, unbounded layered soil, while multi-storey buildings are assumed to be comprised of vertical compressible piers and rigid slabs. Soil-foundation-structure interaction is rigorously taken into account with an affordable number of degrees of freedom. The code allows the direct analysis of multiple piled buildings, so that the influence of other constructions can be taken into account in the analysis of a certain element. The formulation is outlined before presenting validation results and an application example.

## 1 Introduction

The practical interest of understanding the dynamic behaviour of pile foundations becomes evident in view of the large number of related papers published in the last four decades. A highly significant proportion of these works use a boundary element approach to the problem due to the need to model the soil as an unbounded region (see, for example, reviews by Beskos [1, 2] and Padrón [3]). Moreover, most studies focus on the computation of impedances [4, 5, 6], kinematic seismic response [7, 8, 9] or internal forces in pile foundations [10, 11], allowing the analysis of pile-supported structures by means of substructuring strategies. On the contrary, very few works have attempted to tackle the problem using a direct approach in which pile, soil and superstructures are modelled simultaneously [12, 13, 14].

Despite the efforts to analyse pile dynamic response, the influence of nearby pile-supported structures on the behaviour of pile foundations and piled buildings has received, up to the authors' knowledge, no attention at all, except for some preliminary results presented in [15]. For this reason, a direct methodology to study simultaneously soil, piles and several superstructures has been formulated and implemented using the boundary element method to model the layered soil and finite elements for piles and superstructures. This numerical scheme represents an enhancement of a boundary element – finite element coupling model [16] formulated to study pile–soil interaction only. Such a formulation was motivated by the need to develop a flexible and accurate methodology to tackle the problem, and also by the necessity of reducing the meshing

---

\*This is the peer reviewed version of the following article: L.A. Padrón, J.J. Aznárez, O.Maeso, 3-D boundary element–finite element method for the dynamic analysis of piled buildings, *Engineering Analysis with Boundary Elements* 35 (2011) 465–477, which has been published in final form at doi:10.1016/j.enganabound.2010.09.006. This work is released with a Creative Commons Attribution Non-Commercial No Derivatives License.

efforts and the number of degrees of freedom of the model with respect to a multi-domain boundary element approach, as the one used in [17]. In order to meet these requirements, pile-soil interaction forces are modelled as internal loads, pile rigidity is introduced by means of mono-dimensional finite elements, and equilibrium and compatibility conditions are established along the pile axis. Following this strategy, pile-soil interfaces do not need to be discretized by boundary elements leading to a significant reduction in the number of degrees of freedom without appreciably compromising the accuracy of the results.

The boundary element – finite element method formulation for the dynamic analysis of soil-pile-building systems is outlined in section 2. Then, section 3 presents some comparison results in order to check the method and validate its implementation. In order to illustrate the capabilities of the methodology, section 4 shows different types of analyses related to a group of piled buildings in a layered soil subjected to a harmonic excitation applied on the ground surface. Finally, some conclusions and future research directions are provided in the last section. Further details can be found in [3].

## 2 Boundary element – finite element method formulation

In this formulation, the boundary element method is used to model the dynamic behaviour of the stratified soil region, while finite elements are used for piles and superstructures. From the boundary element (soil) point of view, the loads arising from the pile-soil interaction are modelled as distributions of interaction forces applied on an internal line defined by the pile axis, what in this work will be named ‘load-line’ (see figure 1). Piles rigidity is provided by mono-dimensional finite elements, bonded to the surrounding soil by equilibrium and compatibility conditions.

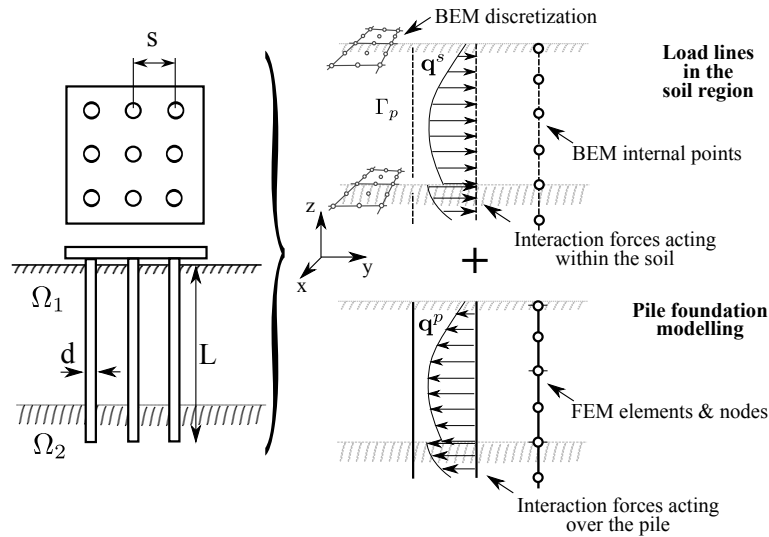


Figure 1: Pile foundation geometry and modelling through BEM-FEM coupling formulation

### 2.1 Pile foundation formulation

Three-node Euler-Bernoulli beam finite elements with axial deformation are used to model the piles. Thirteen degrees of freedom are defined in the element: three orthogonal displacements at each node plus two rotations (torsion excluded) at each one of the end nodes.

The displacement vector  $\mathbf{u}_e(\xi)$  at any point  $\xi$  of an element  $e$  is expressed in terms of the vector of nodal displacements and rotations  $\mathbf{u}_e^p$  as

$$\mathbf{u}_e(\xi) = \Psi(\xi)\mathbf{u}_e^p \quad (1)$$

where  $\Psi(\xi)$  is the matrix of shape functions at point  $\xi$  containing two different sets of functions: (i) a first set of five functions  $\varphi$  used to build an interpolating polynomial of the lateral displacements through the three nodes with explicitly given rotations at both ends; and (ii) a second set of three functions  $\phi$  to approximate the axial deformation. This last set of functions, which correspond to the three Lagrangian polynomials of second order, are also used to approximate the pile-soil contact interaction forces  $\mathbf{q}_e(\xi)$  acting over the pile, within an element  $e$ , as

$$\mathbf{q}_e(\xi) = \mathbf{\Phi}(\xi)\mathbf{q}_e^p \quad (2)$$

where matrix  $\mathbf{\Phi}$  is formed by shape functions  $\phi$  (see [3, 16] for more details) and  $\mathbf{q}_e^p$  is the vector of nodal interaction forces.

The principle of virtual displacements allows to obtain the mass and stiffness matrices ( $\mathbf{M}$  and  $\mathbf{K}$ ) for the described element type [18], and also the matrix  $\mathbf{Q}$  that transforms nodal interaction forces components  $\mathbf{q}^p$  into equivalent nodal forces  $\mathbf{F}^{eq}$  through the linear transformation  $\mathbf{F}_e^{eq} = \mathbf{Q}_e\mathbf{q}_e^p$ .

Hence, after a process of discretization of the pile, computation of elemental matrices and assembly of global matrices, the dynamic behaviour of a certain pile can be represented, in the finite-element sense, by the matrix equation

$$\bar{\mathbf{K}}\mathbf{u}^p = \mathbf{F} + \mathbf{Q}\mathbf{q}^p \quad (3)$$

where the vector of external forces  $\mathbf{F}$  contains the equivalent nodal forces  $\mathbf{F}^{eq}$  from the pile-soil contact interaction, the forces  $\mathbf{F}_{top}$  acting at the top of the pile and the axial force  $\mathbf{F}_p$  at the tip of the pile; where  $\bar{\mathbf{K}} = \mathbf{K} - \omega^2\mathbf{M}$ ,  $\omega$  being the frequency of excitation; and where all matrices must be understood as global to the whole pile.

## 2.2 Soil formulation

In contrast, each stratum  $\Gamma^m$  of the soil is modelled by the BEM as a linear, homogeneous, isotropic, viscoelastic, unbounded region with complex valued shear modulus  $\mu$  of the type  $\mu = Re[\mu](1 + 2i\beta)$ , where  $\beta$  is the damping coefficient and  $i = \sqrt{-1}$ . The boundary integral equation for a time-harmonic elastodynamic state defined in a domain  $\Omega_m$  with boundary  $\Gamma^m$  can be written in a condensed and general form as

$$\mathbf{c}^l\mathbf{u}^l + \int_{\Gamma^m} \mathbf{p}^*\mathbf{u} d\Gamma = \int_{\Gamma^m} \mathbf{u}^*\mathbf{p} d\Gamma + \sum_{j=1}^{n_{ll}^m} \left[ \int_{\Gamma_{p_j}^m} \mathbf{u}^*\mathbf{q}^{sj} d\Gamma_{p_j} - \delta_j \mathbf{\Upsilon}_k^j F_{p_j} \right] \quad (4)$$

where  $\mathbf{c}^l$  is the local free term matrix at collocation point  $\mathbf{x}^l$ ;  $\mathbf{u}$  and  $\mathbf{p}$  are the displacement and traction vectors;  $\mathbf{u}^*$  and  $\mathbf{p}^*$  are the elastodynamic fundamental solution tensors representing the response of an unbounded region to a harmonic concentrated unit load with a time variation  $e^{i\omega t}$  applied at a point  $\mathbf{x}^l$ ;  $\Gamma_{p_j}^m$  is the pile-soil interface along the load-line  $j$  within the domain  $\Omega_m$ ;  $n_{ll}^m$  is the total number of load-lines in the domain  $\Omega_m$ ;  $\delta_j$  is equal to one if the load-line  $j$  contains the tip of a floating pile and zero otherwise;  $\mathbf{\Upsilon}_k^j$  is a three-component vector that represents the contribution of the axial force  $F_{p_j}$  at the tip of the  $j^{th}$  load-line; and  $\mathbf{q}^s = -\mathbf{q}^p$  is the vector of nodal interaction forces acting over the soil, as sketched in figure 1.

The boundaries  $\Gamma^m$  are discretized into quadratic elements of triangular and quadrilateral shapes with six and nine nodes, respectively. Once all boundaries have been discretized, eq. (4) can be written, for each region  $\Omega_m$ , at all nodes on  $\Gamma^m$  in order to obtain a matrix equation of the type

$$\mathbf{H}^{ss}\mathbf{u}^s - \mathbf{G}^{ss}\mathbf{p}^s - \sum_{j=1}^{n_{ll}^m} \mathbf{G}^{sp_j}\mathbf{q}^{sj} + \sum_{j=1}^{n_{ll}^m} \delta_j \mathbf{\Upsilon}^{sj} F_{p_j} = 0 \quad (5)$$

where  $\mathbf{u}^s$  and  $\mathbf{p}^s$  are the vectors of nodal displacements and tractions of boundary elements;  $\mathbf{H}^{ss}$  and  $\mathbf{G}^{ss}$  are coefficient matrices obtained by numerical integration over the boundary elements

of the fundamental solution times the corresponding shape functions; and  $\mathbf{G}^{spj}$  is the coefficient matrix obtained by numerical integration over load-line  $j$  of the fundamental solution times the corresponding interpolation functions, when the unit load is applied on  $\Gamma^m$ .

Furthermore, eq. (4) will be also applied at internal nodes belonging to load-line  $\Gamma_{p_i}^m$ , so that one can write

$$\mathbf{C} \mathbf{u}^{p_i} + \mathbf{H}^{p_i s} \mathbf{u}^s - \mathbf{G}^{p_i s} \mathbf{p}^s - \sum_{j=1}^{n_{ll}^m} \mathbf{G}^{p_i p_j} \mathbf{q}^{s_j} + \sum_{j=1}^{n_{ll}^m} \delta_j \Upsilon^{p_i j} F_{p_j} = 0 \quad (6)$$

where  $\mathbf{H}^{p_i s}$  and  $\mathbf{G}^{p_i s}$  are coefficient matrices obtained by numerical integration over the boundary elements of the fundamental solution times the corresponding shape functions; and  $\mathbf{G}^{p_i p_j}$  is the coefficient matrix obtained by numerical integration over load-line  $j$  of the fundamental solution times the corresponding interpolation functions, when the unit load is applied on load-line  $\Gamma_{p_i}^m$ . Here,  $\mathbf{u}^{p_i}$  is the vector of nodal displacements of the load-line  $i$ , which is multiplied by the diagonal matrix  $\mathbf{C}$ , whose non-zero terms are valued 1/2 in positions corresponding to pile nodes placed on a smooth surface (as e.g. pile heads) and unity at the internal points.

The situation of a pile crossing interfaces between adjacent regions (see figure 1) is worthy of attention. In this case, the distribution of the interaction forces  $\mathbf{q}^s$  along the pile-soil interface is not continuous between layers, and different load-lines are considered in the upper and lower layers. This fact causes a kind of corner problem which can be overcome by applying a non-nodal collocation strategy. For nodes placed on the interface, eq. (6) is applied on an inner point of the pertinent element  $k$ , so that the integral equation becomes

$$\Phi \mathbf{u}_k^{p_i} + \mathbf{H}^{p_i s} \mathbf{u}^s - \mathbf{G}^{p_i s} \mathbf{p}^s - \sum_{j=1}^{n_{ll}^m} \mathbf{G}^{p_i p_j} \mathbf{q}^{s_j} + \sum_{j=1}^{n_{ll}^m} \delta_j \Upsilon^{p_i j} F_{p_j} = 0 \quad (7)$$

where  $\mathbf{u}_k^{p_i}$  is the vector of nodal displacements of element  $\Gamma_k$  and  $\Phi$  is the matrix of shape functions specified at the collocation point.

The axial punctual force  $F_p$  considered at the tip of a floating pile adds a new unknown per pile, in such a way that an extra equation needs to be written. The third row (corresponding to the application of the unit load in the vertical direction) of eq. (7) written for a non-nodal point placed between the two bottom nodes of the pile yields a suitable additional equation for this purpose.

### 2.3 Pile supported structures model

This section describes the adopted formulation for the analysis of the dynamic behaviour of pile-supported multi-storey structures. For this purpose, piles are grouped and fixedly connected

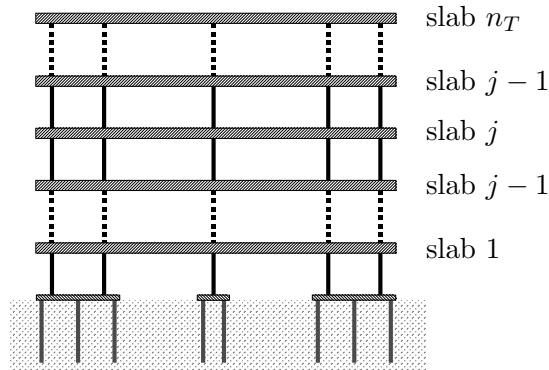


Figure 2: Two-dimensional view of considered pile-supported structures

to rigid pile caps on which the building is founded. The superstructures are assumed to be composed by any number of vertical extensible piers and horizontal rigid slabs (see figure 2). Piers are modelled as massless Euler-Bernoulli beams, with axial and lateral deformation, and with hysteretic damping through a complex valued stiffness of the type  $k = Re[k](1 + 2i\zeta)$ . Torsional stiffness is not considered in the piers. The principal axes of inertia of rigid slabs may have any orientation with respect to the global coordinate axes and, at the same time, the position of their centre of gravity on the horizontal plane can change between storeys, which provides a great deal of generality and flexibility to the model. In order to write the equations directly in terms of slabs displacements and rotations (the most interesting parameters in this kind of study), all DoF at piers ends are condensed to the centre of gravity of slabs and pile caps.

Let  $\mathbf{U}^j = (\{U_1, U_2, U_3, \Theta_1, \Theta_2, \Theta_3\}^j)^T$  be the vector defining displacements and rotations at the centre of gravity of the pile cap or slab  $j$ , and let  $\mathbf{Y}_i^j = (\{u_1, u_2, u_3, \theta_1, \theta_2\}^j)^T$  be the vector defining displacements and rotations at the end of pier or pile  $i$  connected to slab or pile cap  $j$ .

The kinematic relationship between the head of pile  $i$  and the corresponding pile cap  $j$ , or between a pier  $i$  and a certain slab or cap  $j$  can be expressed as

$$\mathbf{Y}_i^j = \mathbf{T}_i^j \mathbf{U}^j \quad (8)$$

where

$$\mathbf{T}_i^j = \begin{bmatrix} 1 & 0 & 0 & 0 & 0 & -(x_{i_2} - x_{cg_2^j}) \\ 0 & 1 & 0 & 0 & 0 & x_{i_1} - x_{cg_1^j} \\ 0 & 0 & 1 & x_{i_2} - x_{cg_2^j} & -(x_{i_1} - x_{cg_1^j}) & 0 \\ 0 & 0 & 0 & 1 & 0 & 0 \\ 0 & 0 & 0 & 0 & 1 & 0 \end{bmatrix} \quad (9)$$

where  $x_{i_1}$  and  $x_{i_2}$  are the  $x_1$  and  $x_2$  coordinates of pier or pile  $i$ , and  $x_{cg_1^j}$  and  $x_{cg_2^j}$  are the  $x_1$  and  $x_2$  coordinates of the centre of gravity of slab or pile cap  $j$ .

On the other hand, the equilibrium at any slab  $j$  can be expressed as

$$\mathbf{F}_{ext}^j + \sum_{i=1}^{n_j} (\mathbf{T}_i^j)^T \mathbf{f}_{i_{top}}^j + \sum_{i=1}^{n_{j+1}} (\mathbf{T}_i^j)^T \mathbf{f}_{i_{bottom}}^{j+1} + \omega^2 \mathbf{M}^j \mathbf{U}^j = 0 \quad (10)$$

where  $\mathbf{F}_{ext}^j$  is the vector of external forces and moments acting on the slab  $j$ ,  $n_j$  is the number of piers in the inter-storey immediately below slab  $j$ ,  $n_{j+1}$  is the number of piers in the inter-storey immediately above slab  $j$ ,  $\mathbf{f}_{i_{top}}^j = (\{f_1, f_2, f_3, m_1, m_2\}^j)^T$  is the vector of forces and moments in the connection between slab  $j$  and pier  $i$  from the inter-storey immediately below,  $\mathbf{f}_{i_{bottom}}^{j+1} = (\{f_1, f_2, f_3, m_1, m_2\}^{j+1})^T$  is the vector of forces and moments in the connection between slab  $j$  and pier  $i$  from the inter-storey immediately above, and

$$\mathbf{M}^j = \begin{bmatrix} M^j \mathbf{I}_{3 \times 3} & \emptyset \\ \emptyset & \mathcal{I} \end{bmatrix} \quad (11)$$

where  $M^j$  is the mass of the slab,  $\mathbf{I}_{3 \times 3}$  is the identity matrix of order 3, and  $\mathcal{I}$  is the  $3 \times 3$  tensor expressing the slab moments of inertia.

As mentioned above, piers are modelled as massless Euler-Bernoulli beams with axial deformation. In this way, and in the absence of external forces applied along the pier, the relationship between forces and displacements at both ends of the pier is given by a  $10 \times 10$  stiffness matrix of the form

$$\begin{bmatrix} \mathbf{f}_{i^b} \\ \mathbf{f}_{i^t} \end{bmatrix}^j = \begin{bmatrix} \mathbf{K}_i^{bb} & \mathbf{K}_i^{bt} \\ \mathbf{K}_i^{tb} & \mathbf{K}_i^{tt} \end{bmatrix}^j \begin{bmatrix} \mathbf{Y}_{i^b} \\ \mathbf{Y}_{i^t} \end{bmatrix}^j \quad (12)$$

where  $b$  and  $t$  stand for *bottom* and *top* respectively.

By substitution of (12) into (10), and taking (8) into account, the equilibrium equation for slab  $j$  can be written as

$$\mathbf{F}_{ext}^j + \mathbf{K}_{j,j-1} \mathbf{U}^{j-1} + (\omega^2 \mathbf{M}^j + \mathbf{K}_{j,j}) \mathbf{U}^j + \mathbf{K}_{j,j+1} \mathbf{U}^{j+1} = 0 \quad (13)$$

where

$$\mathbf{K}_{j,j} = \sum_{i=1}^{n_j} (\mathbf{T}_i^j)^T \mathbf{K}_i^{tt^j} \mathbf{T}_i^j + \sum_{i=1}^{n_{j+1}} (\mathbf{T}_i^j)^T \mathbf{K}_i^{bb^{j+1}} \mathbf{T}_i^j \quad (14)$$

$$\mathbf{K}_{j,j-1} = \sum_{i=1}^{n_j} (\mathbf{T}_i^j)^T \mathbf{K}_i^{tb^j} \mathbf{T}_i^{j-1} \quad (15)$$

$$\mathbf{K}_{j,j+1} = \sum_{i=1}^{n_j} (\mathbf{T}_i^j)^T \mathbf{K}_i^{bt^{j+1}} \mathbf{T}_i^{j+1} \quad (16)$$

These submatrices represent the three terms of the superstructure stiffness matrix that appear in the row corresponding to slab  $j$ , and where the contribution of all piers in each storey above and below such a slab is taken into account.

On the other hand, an equation equivalent to (10) can be written for each of the pile caps on which the superstructure is founded. To express such an equilibrium equation in the format of eq. (13), eq. (3) must be rewritten for the top element of pile  $i$  in terms of submatrices affecting either the pile head node or the other two underground nodes of the element as

$$\begin{bmatrix} 5 \times 5 \bar{\mathbf{K}}^{hh} & 5 \times 8 \bar{\mathbf{K}}^{hu} \\ 8 \times 5 \bar{\mathbf{K}}^{uh} & 8 \times 8 \bar{\mathbf{K}}^{uu} \end{bmatrix}_i \begin{bmatrix} \mathbf{u}^h \\ \mathbf{u}^u \end{bmatrix}_i + \begin{bmatrix} 5 \times 9 \mathbf{Q}^h \\ 8 \times 9 \mathbf{Q}^u \end{bmatrix}_i \mathbf{q}^{s_i} = \begin{bmatrix} \mathbf{f}^h \\ \mathbf{f}^u \end{bmatrix}_i \quad (17)$$

where  $h$  and  $u$  stand for *head* and *underground* respectively, and where the dimensions of the submatrices are written on its top left side. Then, the forces at the top of the pile, equivalent to the term  $\mathbf{f}_{i,top}^j$  of eq. (10), can be obtained as

$$\mathbf{f}^h = \bar{\mathbf{K}}_i^{hh} \mathbf{u}_i^h + \bar{\mathbf{K}}_i^{hu} \mathbf{u}_i^u + \mathbf{Q}_i^h \mathbf{q}^{s_i} \quad (18)$$

which, taking eq. (8) into account, allows us to express the equilibrium equation at a certain pile cap  $c$  as

$$\mathbf{F}_{ext}^c + \mathbf{K}_{c,1} \mathbf{U}^1 + (\omega^2 \mathbf{M}^c + \mathbf{K}_{c,c}) \mathbf{U}^c + \sum_{i=1}^{n_{piles}^c} \left( \tilde{\mathbf{K}}_{c,i} \mathbf{u}_i^u + \tilde{\mathbf{Q}}_{c,i} \mathbf{q}^{s_i} \right) = 0 \quad (19)$$

where

$$\mathbf{K}_{c,1} = \sum_{i=1}^{n_1} (\mathbf{T}_i^c)^T \mathbf{K}_i^{bt^1} \mathbf{T}_i^1 \quad (20)$$

$$\mathbf{K}_{c,c} = \sum_{i=1}^{n_{piles}^c} (\mathbf{T}_i^c)^T \bar{\mathbf{K}}_i^{hh} \mathbf{T}_i^c + \sum_{i=1}^{n_1} (\mathbf{T}_i^c)^T \mathbf{K}_i^{bb^1} \mathbf{T}_i^c \quad (21)$$

$$\tilde{\mathbf{K}}_{c,i} = (\mathbf{T}_i^c)^T \bar{\mathbf{K}}_i^{hu} \quad (22)$$

$$\tilde{\mathbf{Q}}_{c,i} = (\mathbf{T}_i^c)^T \mathbf{Q}_i^h \quad (23)$$

## 2.4 Seismic excitation modelling

The system described in the previous sections can be excited either by forced displacements prescribed at certain points, by applied external forces or by a far-source earthquake. This section discusses how this last kind of action is modelled.

When seismic waves impinge on the site under study, reflection and refraction phenomena take place, and the arising wave field modifies the incident wave train. The original wave field, which is assumed to come from a far away source, is the *incident field*  $\mathbf{u}_I$ , while the one produced by the reflection and refraction phenomena receives the name of *scattered field*  $\mathbf{u}_S$ . The resulting displacement and traction fields (*total fields*) can be obtained by superposition as  $\mathbf{u} = \mathbf{u}_I + \mathbf{u}_S$  and  $\mathbf{p} = \mathbf{p}_I + \mathbf{p}_S$ .

Let us consider that a pile foundation embedded in a layered soil is subjected to time-harmonic incident waves. In this case, eq. (5) represents the discretized boundary integral equation for each region  $\Gamma_m$  in terms of the total field. On the other hand, as the incident, scattered and total fields satisfy the governing equations, such an equation can also be written in terms of the incident field as

$$\mathbf{H}^{ss}\mathbf{u}_I^s - \mathbf{G}^{ss}\mathbf{p}_I^s = 0 \quad (24)$$

where interaction forces along the pile-soil interface  $\mathbf{q}^{sj}$  and forces at piles tip  $F_{p_j}$  are not present because they only exist in the scattered fields. The subtraction of eq. (24) from eq. (5) yields

$$\mathbf{H}^{ss}\mathbf{u}^s - \mathbf{G}^{ss}\mathbf{p}^s - \sum_{j=1}^{n_l^m} \mathbf{G}^{spj}\mathbf{q}^{sj} + \sum_{j=1}^{n_l^m} \delta_j \Upsilon^{sj} F_{p_j} = \mathbf{H}^{ss}\mathbf{u}_I^s - \mathbf{G}^{ss}\mathbf{p}_I^s \quad (25)$$

where the right-hand vector is known because the analytic expressions of  $\mathbf{u}_I^s$  and  $\mathbf{p}_I^s$  can be easily obtained. The same procedure can be repeated to obtain the BE equations (6) and (7) for load-lines. In contrast, the pile FE eq. (3) holds true for the total fields and, therefore, does not need to be rewritten. Finally, note that the magnitude of the scattered field decreases with distance due to the existing material and radiation damping in the soil, and consequently, boundaries far from the pile foundation do not need to be discretized.

## 2.5 Assembly of the global system matrix of equations

Equations (3), (5), (6), (7), (13) and (19) (or the corresponding equations for incident seismic fields, if it were the case) can be arranged to form a linear system of equations representing a general problem consisting on a certain number of superstructures, each founded on one or more caps, each one of which groups two or more different piles embedded in a viscoelastic soil of generic stratigraphy and topography. Equilibrium and compatibility fully-bonded contact conditions over the different interfaces of the problem are imposed. The most general situation is that of a problem with multiple superstructures founded on different pile caps on a layered soil, the system being subject to external forces and/or incident seismic waves. In such a general case, the system of equations is of the form

$$\mathcal{A} \{ \mathbf{u}^s, \mathbf{p}^s, \mathbf{q}^s, \mathbf{F}_p, \mathbf{u}^p, \mathbf{U}^j \}^T = \mathcal{B} \quad (26)$$

where  $\mathcal{A}$ , whose structure is sketched in figure 3, is the square matrix of coefficients and  $\mathcal{B}$  is the known vector, both computed by rearranging the equations and prescribing the known boundary conditions. The vector of unknowns includes the displacements  $\mathbf{u}^s$  and/or tractions  $\mathbf{p}^s$  at boundary element nodes, the interaction forces at pile-soil interface  $\mathbf{q}^s$ , the forces at pile tips  $\mathbf{F}_p$ , the nodal translations and rotations at pile nodes  $\mathbf{u}^p$ , and the degrees of freedom defined at the structures  $\mathbf{U}^j$ .

Note that the displacements at the pile head nodes have been condensed and that the first five equations of expression (3) have been included in (19) in such a way that only the equations corresponding to underground nodes have to be written in the form of eq. (3).

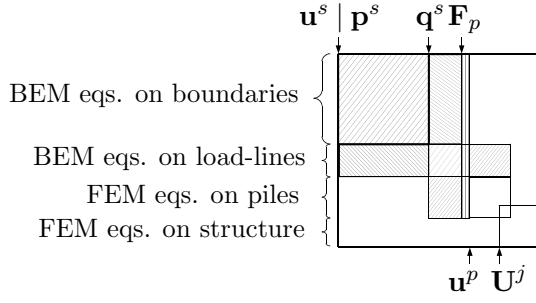


Figure 3: Structure of the system matrix of coefficients  $\mathcal{A}$

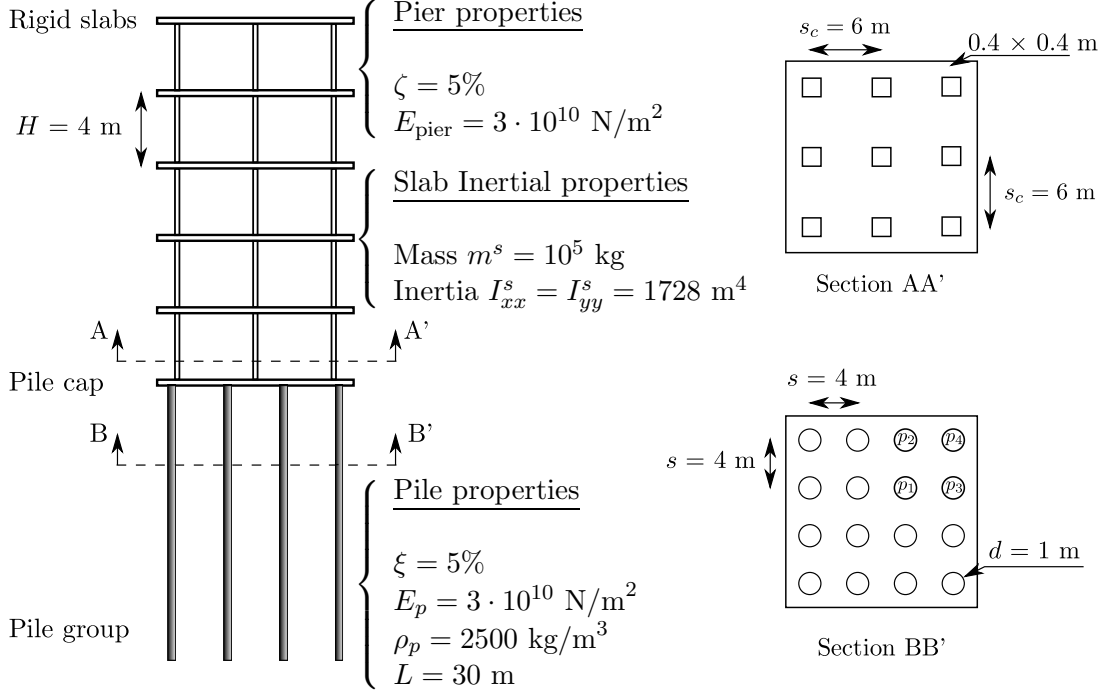


Figure 4: Two-dimensional sketch of considered pile-supported structures

### 3 Validation results

As mentioned in the introduction, the formulation proposed in this work represents an enhancement of a work presented a few years ago for the dynamic analysis of pile foundations exclusively [16]. This part of the formulation, related only to the response of the foundation, has been thoroughly validated [16, 3]. This section intends to validate the whole soil-foundation-building formulation by comparing results obtained from the direct methodology presented herein against results from a substructuring approach.

The example used for this purpose is depicted in figure 4, where a small five-storey RC building founded on a group of 16 piles is sketched. The system is modelled through five rigid slabs, nine  $0.4 \times 0.4 \text{ m}$  vertical piers per storey, and a rigid pile cap for the  $4 \times 4$  pile group embedded in a homogeneous half-space. The main structural properties are included in the figure, while the soil properties are: soil internal damping coefficient  $\beta = 0.05$ , soil density  $\rho_s = 1750 \text{ kg/m}^3$ , soil Poisson's ratio  $\nu_s = 0.4$  and shear wave velocity  $c_s = 239 \text{ m/s}$ . These data yield a pile-soil modulus ratio  $E_p/E_s = 107.1$ .

### 3.1 Substructuring model

Regarding the substructuring approach, a two-dimensional model of the system is used, with 2 degrees of freedom (horizontal displacement and rotation) per slab and also on the pile cap. The stiffness matrices, damping properties, inertial features and input motions characterizing the system must be defined for the specific case at hand. In this way, for each storey of the building described above, and modelling piers as compressible Euler-Bernoulli beams, the stiffness submatrix  $\mathcal{K}_{ij}^s$  between slabs  $i$  (upper slab, first two DoF) and  $j$  (lower slab, second two DoF) is defined as

$$\mathcal{K}_{ij}^s = \begin{pmatrix} k_{11} & -k_{12} & -k_{11} & -k_{12} \\ -k_{12} & k_{22} + k_a & k_{12} & k_{22}/2 - k_a \\ -k_{11} & k_{12} & k_{11} & k_{12} \\ -k_{12} & k_{22}/2 - k_a & k_{12} & k_{22} + k_a \end{pmatrix}_{ij} \quad (27)$$

where  $k_{11} = 9 \cdot 12(EI)_{\text{pier}}/H^3$ ,  $k_{12} = 9 \cdot 6(EI)_{\text{pier}}/H^2$ ,  $k_{22} = 9 \cdot 4(EI)_{\text{pier}}/H$  and  $k_a = 6 \cdot (EA)_{\text{pier}}s_c/L$ ,  $A_{\text{pier}}$  and  $I_{\text{pier}}$  being the area and inertia of the pier section,  $E_{\text{pier}}$  the modulus of elasticity, and  $H$  the pier height. In order to include hysteretic damping in the model, all the elements of matrix  $\mathcal{K}_{ij}^s$  are complex numbers of the type  $k = Re[k](1 + 2i\zeta)$ .

The dynamic stiffness of the foundation (where two DoF are also considered) is assumed to be defined by swaying ( $K_{xx} = k_{xx} + ia_0c_{xx}$ ), rocking ( $K_{\theta\theta} = k_{\theta\theta} + ia_0c_{\theta\theta}$ ) and the crossed horizontal-rocking ( $K_{x\theta} = k_{x\theta} + ia_0c_{x\theta}$ ) impedance functions, where  $k_{ij}$  and  $c_{ij}$  are the frequency dependent dynamic stiffness and damping coefficients, respectively,  $a_0 = \omega d/c_s$  is the dimensionless frequency and  $c_s$  is the soil shear-wave velocity. Therefore, the stiffness matrix of the pile foundation can be written as

$$\mathcal{K}^f = \begin{pmatrix} K_{xx} & K_{x\theta} \\ K_{x\theta} & K_{\theta\theta} \end{pmatrix} \quad (28)$$

Such impedance functions have been computed for our particular case as specified in [16], and are shown in figure 5.

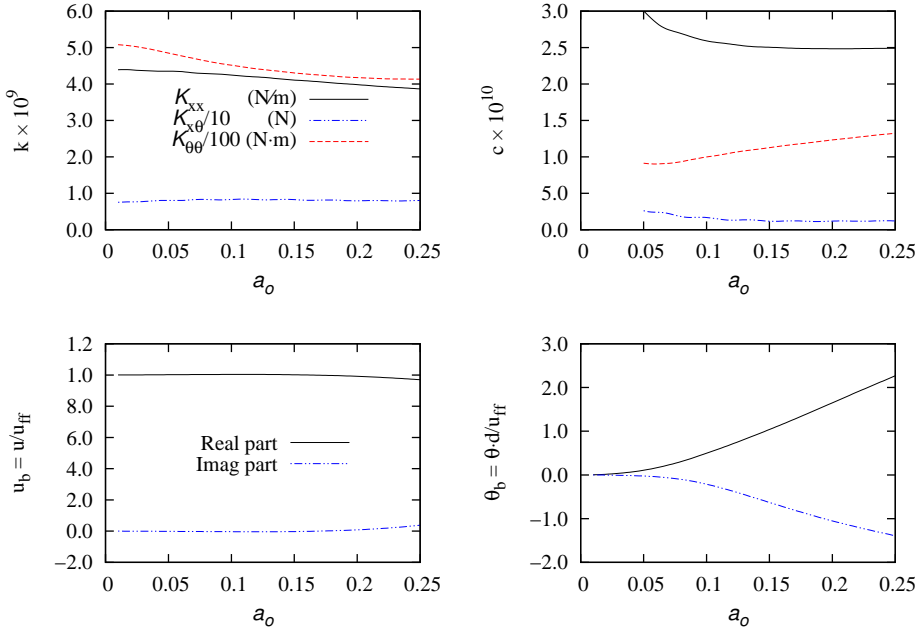


Figure 5: Dynamic stiffness (top) and kinematic interaction (bottom) functions of  $4 \times 4$  pile group

Having defined the stiffness matrices  $\mathcal{K}^s$  and  $\mathcal{K}^f$  for building storeys and foundation respectively, and having all DoF condensed to the slabs and cap centres of gravity, the twelve-DoF stiffness matrix  $\mathcal{K}$  for the entire system defined at the beginning of this section can be obtained following the classic assembly process of the direct stiffness method.

On the other hand, figure 5 contains also the translational ( $u_b = u/u_{ff}$ ) and rotational ( $\theta_b = \theta \cdot d/u_{ff}$ ) kinematic interaction functions of the soil-foundation system impinged by vertically-incident S waves. These functions represent the horizontal and rotational motions induced in the foundation by the seismic actions in the absence of a superstructure, and related to the horizontal motion ( $u_{ff}$ ) produced in the surface of the far-field soil (undisturbed by the presence of the foundation) by the same incident seismic waves. These functions define the input motion through a vector  $\mathbf{U}_b$  of appropriate dimensions ( $12 \times 1$  in this case), having only two non-zero terms.

The mass is assumed to be concentrated on slabs and pile caps, in such a way that the system inertial properties are defined by a submatrix of the form

$$\mathcal{M}_i = \begin{pmatrix} m_i & 0 \\ 0 & I_i \end{pmatrix} \quad (29)$$

where  $m_i$  and  $I_i$  are the mass and moment of inertia (with respect to a horizontal axis perpendicular to the paper and passing through the centre of gravity of the slab) for every slab or for the pile cap. As usual, this submatrix is used to define the mass matrix  $\mathcal{M}$  of the system.

Finally, the dynamic response of the system can be evaluated through an equation of motion of the type

$$(\mathcal{K} - \omega^2 \mathcal{M}) \mathbf{U} = \hat{\mathcal{K}}^f \mathbf{U}_b \quad (30)$$

where  $\mathbf{U}$  is a complex vector that contains displacements and rotations at slabs and pile cap, and  $\hat{\mathcal{K}}^f$  is a  $12 \times 12$  zero matrix into which  $\mathcal{K}^f$  is placed in the appropriate position.

### 3.2 Comparison results

The dynamic response of the system defined at the beginning of this section and subjected to vertically-incident S waves can now be obtained both by the direct methodology (as explained in section 2) and by the substructuring approach (building equation (30) for the system at hand and with the input data given in figure 5). Figure 6 presents a comparison between results obtained from both methodologies in terms of the real and imaginary horizontal displacements arising at each slab, together with a measure of the relative difference between them. It can be seen that both groups of results are in very good agreement.

## 4 Application example

In order to explore the possibilities of the boundary-element code presented in this work, results for the problem sketched in figure 7 are going to be discussed in this section. Soil profile, pile foundations and superstructures have been defined with rather regular and simplified characteristics in order to obtain easily interpretable results, allowing an assessment of the model. Note, however, that regarding the code capabilities, the buildings could have been irregular and different among them, the soil profile could have been defined by any number of non-horizontal and non-planar surfaces, a larger number of superstructures could have been studied, or a different kind of excitation could have been used.

As shown in figure 7, two cases are going to be considered, with either one or three structures. The focus of the discussion will be on how the dynamic response of the piled building of case A is affected by the presence of the additional structures introduced in case B. Unlike the validation case, in which the system was subjected to seismic waves, a vertical forced displacement  $u_f$  applied on a rectangular portion of the ground surface has been considered. In the horizontal

directions, zero-traction boundary conditions have been imposed. The figure shows the distance ( $b$  being the foundation half-width) between buildings and to the area (of dimensions  $b \times 2b$ ) where vertical displacements are forced.

The properties of the pile group and the superstructures are the ones defined in section 3 for the validation example. In this case, however, the buildings are founded on a soft stratum overlying a stiff half-space. The properties of the soil deposit are: soil internal damping coefficient  $\beta_d = 0.05$ , soil density  $\rho_d = 1750 \text{ kg/m}^3$ , soil Poisson's ratio  $\nu_d = 0.4$ , shear wave velocity  $c_{sd} = 239 \text{ m/s}$  and thickness  $H_d = 24 \text{ m}$ . On the other hand, the properties of the underlying half-space are:  $\beta_h = 0.05$ ,  $\rho_h = 2100 \text{ kg/m}^3$ ,  $\nu_h = 0.3$  and  $c_{sh} = 690 \text{ m/s}$ .

The domain boundaries have been discretized into quadratic elements of triangular and quadrilateral shapes. A representation of the mesh is shown in figure 8, where piles, buildings and excitation area are also included. The symmetry of the problem allows the discretization of only one quarter of the system. Identical meshes have been used for both the domain interface and the ground surface, a top view of which has been placed at the right-bottom corner of the figure. Note that the magnitudes of the displacements and tractions decrease with distance due to the existing material and radiation damping in the soil and, consequently, boundaries far from the area of interest do not need to be included in the discretization. The extension and topology of the boundary element mesh have been established through sensitivity analyses. In case B, for instance, the mesh (shown in figure 8) contains 6139 boundary elements and 384 pile finite elements, leading to a system of equations with 27741 degrees of freedom.

Three different types of results will be shown in the next subsections: *a*) internal forces in piles, *b*) ground surface and pile cap displacements, and *c*) relative lateral displacements between two consecutive floors as inter-storey drift.

The dynamic response of the system has been studied in the range of interest  $0 < a_o \leq 0.25$ , in which the first three natural frequencies of the structures are located. As shown in figure 9, where the absolute horizontal displacements of the floors are shown for case A, such natural frequencies occur for  $a_o \simeq 0.045$ ,  $0.13$  and  $0.21$ .

#### 4.1 Internal forces in piles

Figures 10, 11 and 12 present envelopes of bending moment, shear forces and axial forces, respectively, for four piles belonging to the central structure (the one present both in cases A and B). Such piles are labelled as defined in figure 4, and results are shown for cases A and B together in order to make apparent the influence of the presence of other buildings. Indeed, maximum internal forces always occur when the structure under study is alone. As expected, maximum values are found at pile heads and at the interface between the soft deposit and the stiffer half-space. At these depths, differences are, in general, more important. Also, piles  $p_3$  and  $p_4$ , placed on the side looking towards the area where the loads are applied, carry the greatest loads, while pile  $p_1$ , being one of the 'internal' piles, takes always the smaller loads. Note, however, that bending moments and shear forces at the domain interface are, as expected, of the same order of magnitude for all piles in the group due to the fact that they are produced mainly by kinematic interaction.

The right sides of figures 10, 11 and 12 show the frequencies at which the maximum internal forces at each point (presented on the left side) take place. It can be seen that all values in the envelopes correspond to values of  $a_o > 0.13$ , that is, for frequencies above the second natural frequency of the building-foundation-soil systems.

#### 4.2 Ground surface and pile cap displacements

Figures 13 and 14 present horizontal and vertical displacements, respectively, at five different points on the ground surface: point  $x = 0$  (see figure 7) just below the central building; point  $x = 1.5b$  between the central structure and the one near the area where the excitation is applied; point  $x = 3b$  just below the lateral building near the forced-displacement area; and points

$x = 4.5b$  and  $x = 6b$  between the lateral building and the area where the excitation is defined. Displacements are given in terms of real and imaginary parts for cases A and B together with the situation in which neither structures nor foundations are built.

As expected, the dynamic amplifications for both horizontal and vertical displacements begin to be significant after the natural frequency of the deposit, which can be easily shown to be  $a_{o_d} = \pi/48 \simeq 0.065$ . Also, the presence of the central building (case A) has very little influence on the response of points  $x = 4.5b$  and  $x = 6b$  in comparison to the situation without any constructions. In contrast, the introduction of additional buildings (case B) reduce very significantly the magnitude of the ground displacements when  $x \leq 4.5b$  for  $a_o \gtrsim 0.12$ , frequency from which the half-wave length on the ground surface begins to be of the same order of magnitude of the distance covered by two adjacent buildings, thus restraining the ground surface deformed shape. On the other hand, the natural frequencies of the building-foundation-soil systems do not have a significant impact on the dynamic response of the ground surface in this configuration.

Figure 15 shows horizontal displacements and rotations measured at the pile cap of the central structure for both cases A and B. Real and imaginary parts are presented. It can be seen that the presence of the other buildings influences strongly the dynamic response of the structure under study, as the magnitude of both displacements and rotations is reduced by approximately 50%. Indeed, the lateral buildings block the waves in the soil, reducing the vibrations measured at the central building, mainly for  $a_o \gtrsim 0.12$  as commented above. On the other hand, the fundamental frequency of the deposit associated with S waves is clearly marked in the plot representing the horizontal displacement of the cap, as there is a maximum of the real part and an inflection point in the imaginary part at such a frequency.

### 4.3 Inter-storey drift

The maximum shear deformation to be withstood by piers in a floor are analysed in this section in terms of the inter-storey drift. Figure 16 presents the inter-storey drifts in each floor of the central building for both cases A and B. On the other hand, figure 17 represents an envelope of maximum relative displacements. The floor at which each maximum occurs is represented in colours according to the legend.

As expected, maximum values correspond to case A (one building only), although there is no difference between both cases for frequencies below  $a_o = 0.1$ . It can be seen that the largest relative displacements occur for the second and third modes of vibration in the buildings, with frequencies above the fundamental period of the soil deposit. When the observed building is alone, inter-storey drifts are significantly larger around the third fundamental frequency, while for case B, relative displacement magnitudes around second and third modes are of similar order, although maxima occur at different floors in each case. As usual, the largest inter-storey drifts around the first and second natural frequencies correspond to the first floor while, in the case of the third natural frequency, the largest values are found in the third floor, such a behaviour being similar for cases A and B.

## 5 Summary and conclusions

A numerical scheme is presented for the three-dimensional dynamic analysis of piled buildings in the frequency domain taking soil-foundation-structure interaction rigorously into account. In the proposed formulation, piles are modelled as compressible Euler-Bernoulli beams founded on a linear, isotropic, viscoelastic, zoned-homogeneous, unbounded layered soil, while multi-storey buildings are assumed to be comprised of vertical compressible piers and rigid slabs.

The boundary element method is used to model the different layers or regions forming the soil profile. The problem is formulated so that soil-pile interface does not need to be discretized with boundary elements. Instead, the pile-soil interaction forces are assumed to act on a line defined by the pile axis and, at the same time, the foundation rigidity is provided by mono-dimensional

beam linear finite elements used to represent the piles. Compatibility in displacements is set between the pile finite element nodes and the corresponding soil points considered as internal boundary element points. Equilibrium conditions are also imposed along the pile axes between the internal ‘load lines’ acting within the soil and the corresponding interaction forces acting over the piles. With this strategy, pile group harmonic response can be accurately computed taking into account the actual stiffness of piles and soil, together with the pile-soil interaction effects, while the total number of degrees of freedom is significantly reduced with respect to a multi-domain boundary element approach. Then, piles are linked through rigid caps to form the different pile groups on which the buildings are going to be founded. Finally, condensed stiffness and mass matrices representing the superstructures are computed, the displacements and rotations at the centre of gravity of slabs and pile caps being the degrees of freedom of interest in the buildings. Rigid slabs may have any orientation within the horizontal plane and, at the same time, the position of their centre of gravity on the horizontal plane can change between storeys. The number, properties and position of the piers can also change from one floor to the next. All these features provide a great generality and flexibility to the model.

This novel methodology is useful in the analysis of structure-soil-structure interaction problems for piled buildings. It can be used to study, for instance, the seismic response of groups of buildings, the effects of nearby constructions on the dynamic response of a building, or vibrations induced in a building by dynamic actions able to generate waves propagating in the soil and interacting with obstacles and other constructions. The novelty of the proposed scheme resides in the treatment of the soil-foundation interaction and the generality of the code that allows the direct analysis of multiple piled buildings in layered soils simultaneously, without substructuring strategies involved.

A validation case, corresponding to a five-storey piled building subjected to vertically-incident S waves, is presented to show the accuracy of the code compared to results obtained following a substructuring approach. In order to show the flexibility and the possibilities of the numerical scheme, different results are presented to study the vibrations induced by a harmonic excitation acting on the ground surface near a group of piled buildings. The dynamic response on ground surface, pile foundations and superstructures is analysed for only one building or for a group of three, focusing on the influence of additional structures on the observed building and the surrounding soil.

The model presented in this paper can be enhanced in a number of different ways. For instance: (a) generalization of the pile finite element formulation for general curvilinear elements, so that structural typologies other than vertical piles can be analysed; (b) implementation of incident seismic waves with any direction of incidence, so that the effects of such a parameter on the seismic response of pile foundations and pile-supported structures can be assessed; (c) formulation of a numerical scheme able to model the interaction between pile and surrounding water, i.e. between a pile and a potential region, which would lead to a more general formulation able to model, for instance, the dynamic behaviour of a pile embedded in a poroelastic soil; (d) modelling of a pile raft foundation by means of thin plate/shell finite elements, allowing the analysis of very large pile groups for which the assumption of rigidity of the pile cap is not generally acceptable; or (e) generalization of the superstructure model with new types of elements, such as shear walls, inclined elements, flexible slabs and beams.

## Acknowledgements

This work was supported by the Spanish Ministry of Science and Innovation (Secretaría de Estado de Investigación) through research project BIA2007-67612-C02-01 and co-financed by the European Fund of Regional Development. The authors are indebted to an anonymous reviewer whose comments and suggestions contributed to improve the paper.

## References

- [1] D E Beskos. Boundary element methods in dynamic analysis. *Appl Mech Rev*, 40:1–23, 1987.
- [2] D E Beskos. Boundary element methods in dynamic analysis: Part II (1986-1996). *Appl Mech Rev*, 50:149–197, 1997.
- [3] L A Padrón. *Numerical model for the dynamic analysis of pile foundations*. PhD thesis, University of Las Palmas de Gran Canaria (available for download at <http://acceda.ulpgc.es/handle/10553/2841>), 2009.
- [4] R Sen, T G Davies, and P K Banerjee. Dynamic analysis of piles and pile groups embedded in homogeneous soils. *Earthquake Eng Struct Dyn*, 13:53–65, 1985.
- [5] A M Kaynia and E Kausel. Dynamics of piles and pile groups in layered soil media. *Soil Dyn Earthquake Eng*, 10:386–401, 1991.
- [6] K Miura, A M Kaynia, K Masuda, E Kitamura, and Y Seto. Dynamic behaviour of pile foundations in homogeneous and non-homogeneous media. *Earthquake Eng Struct Dyn*, 23(2):183–192, 1994.
- [7] S M Mamoon and P K Banerjee. Response of piles and pile groups to travelling sh-waves. *Earthquake Eng Struct Dyn*, 19:597–610, 1990.
- [8] S M Mamoon and S Ahmad. Seismic response of piles to obliquely incident sh, sv and p waves. *J Geotech Eng, ASCE*, 116(2):186–204, 1990.
- [9] A M Kaynia and M Novak. Response of pile foundations to rayleigh waves and obliquely incident body waves. *Earthquake Eng Struct Dyn*, 21:303–318, 1992.
- [10] A M Kaynia and S Mahzooni. Forces in pile foundations under seismic loading. *J Eng Mech, ASCE*, 122:46–53, 1996.
- [11] H Masayuki and N Shoichi. A study on pile forces of a pile group in layered soil under seismic loadings. In *Proc. of the II Int Conf on Recent Advances in Geotech Earthquake Eng and Soil Dyn*, St Louis, Missouri, 1991.
- [12] J Guin and P K Banerjee. Coupled soil-pile-structure interaction analysis under seismic excitation. *J Struct Eng*, 124(4):434–444, 1998.
- [13] J Guin. *Advanced soil-pile-structure interaction and nonlinear behavior*. PhD thesis, State University of New York, Buffalo, 1997.
- [14] K K Koo, K T Chau, X Yang, S S Lam, and Y L Wong. Soil-pile-structure interaction under SH wave excitation. *Earthquake Eng Struct Dyn*, 32:395–415, 2003.
- [15] L A Padrón, J J Aznárez, and O. Maeso. Dynamic structure-soil-structure interaction between nearby piled buildings under seismic excitation by BEM-FEM model. *Soil Dyn Earthquake Eng*, pages 1084–1096, 2009.
- [16] L A Padrón, J J Aznárez, and O. Maeso. BEM-FEM coupling model for the dynamic analysis of piles and pile groups. *Eng Anal Bound Elem*, 31:473–484, 2007.
- [17] O Maeso, J J Aznárez, and F García. Dynamic impedances of piles and groups of piles in saturated soils. *Comput Struct*, 83:769–782, 2005.
- [18] R W Clough and J Penzien. *Dynamics of structures*. McGraw-Hill, 1982.

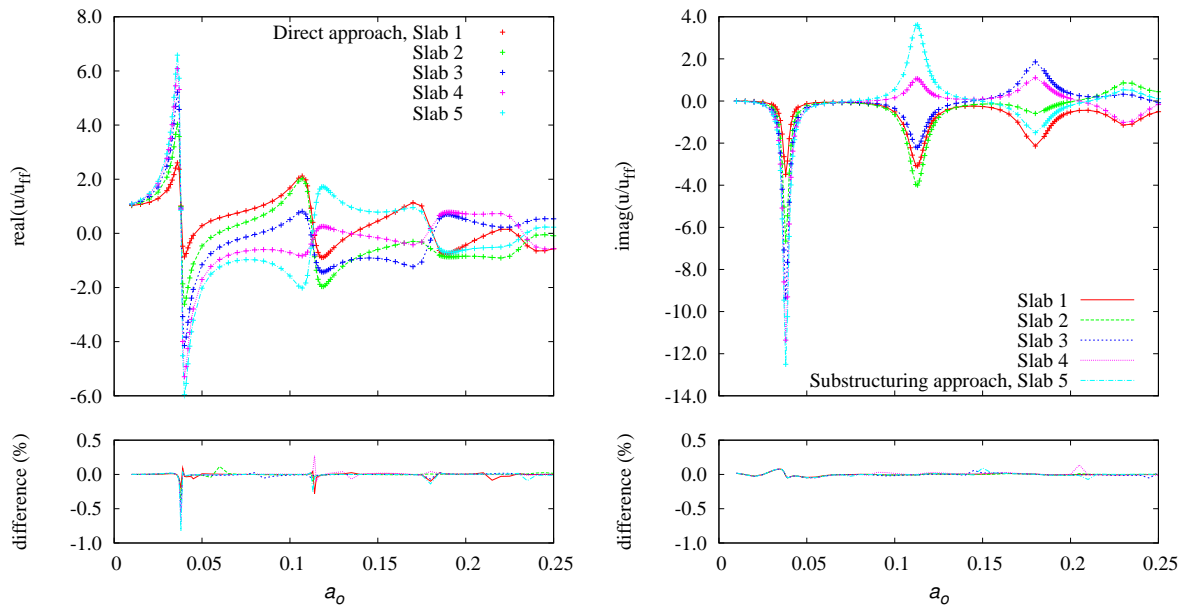


Figure 6: Comparison results between substructuring (lines) and direct (points) approaches

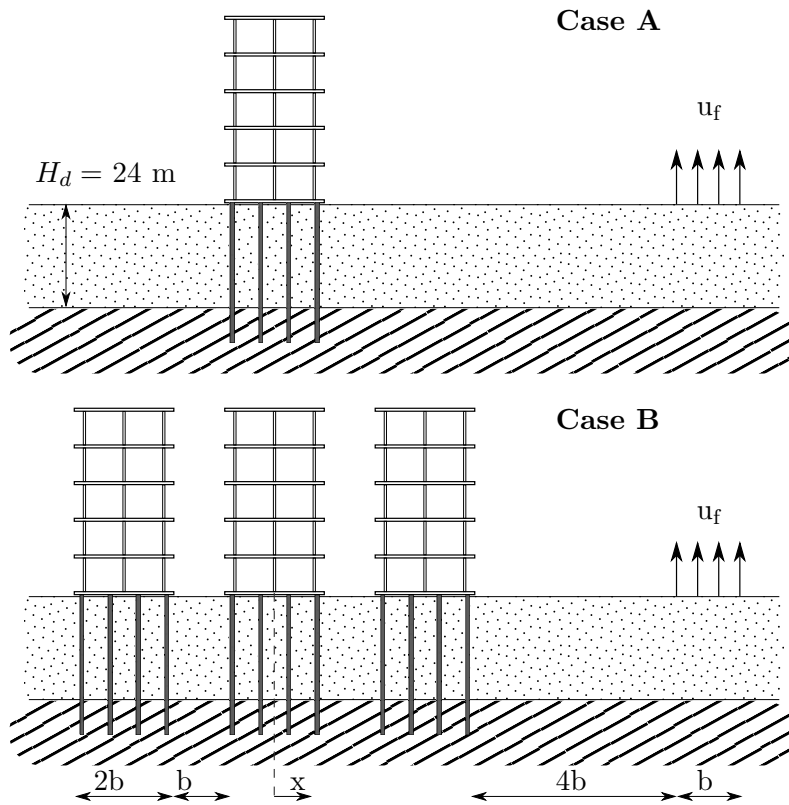


Figure 7: Application example description

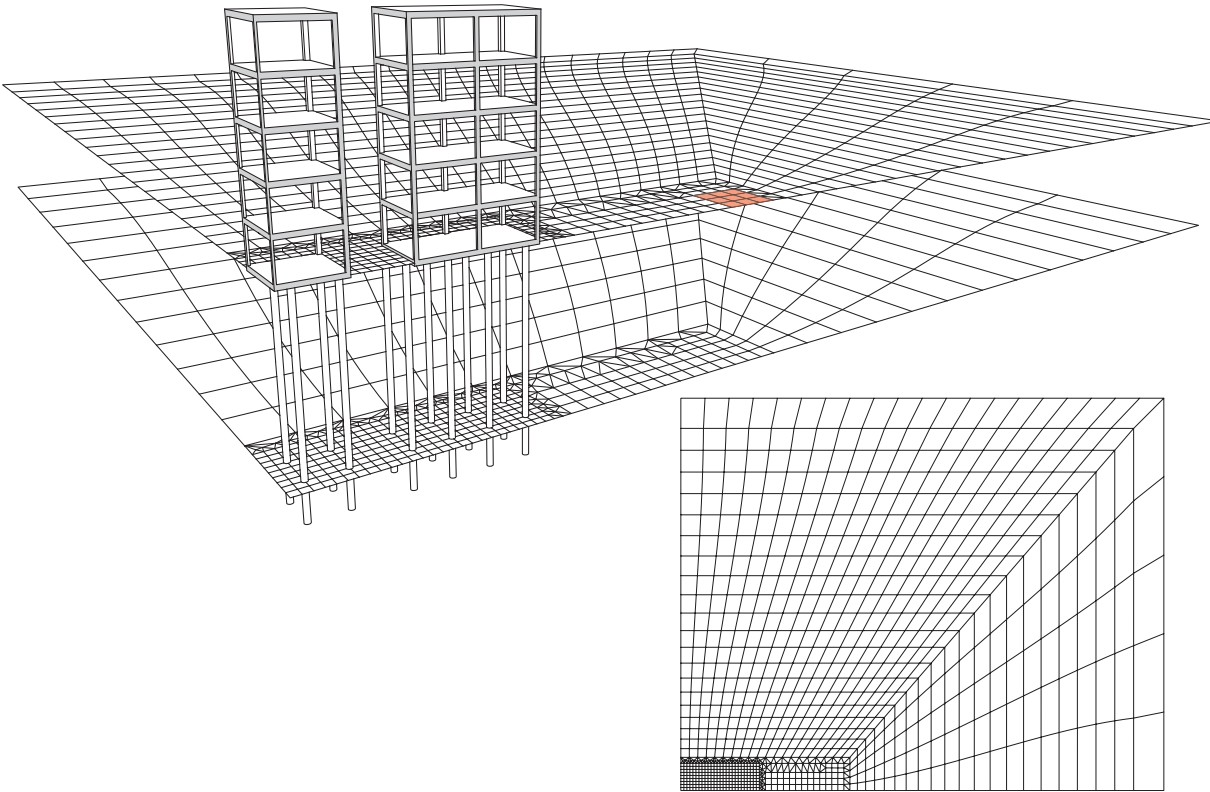


Figure 8: Representation of the mesh (modelling a quarter of the geometry) used for computations. The area where excitation is applied is marked in red in the upper illustration.

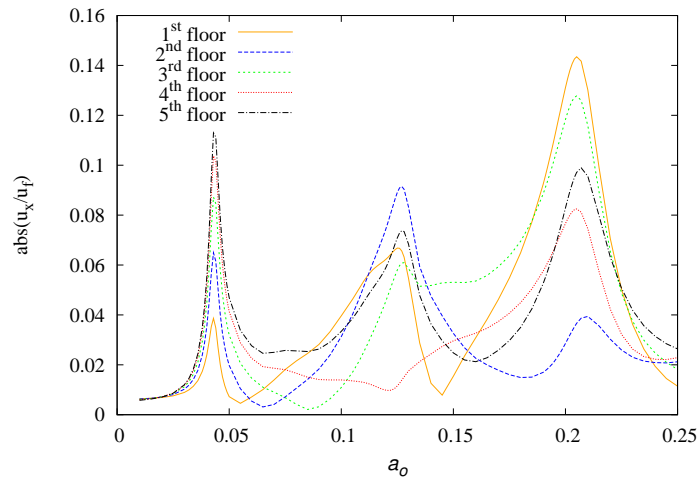


Figure 9: Absolute horizontal displacements in floor slabs for case A.

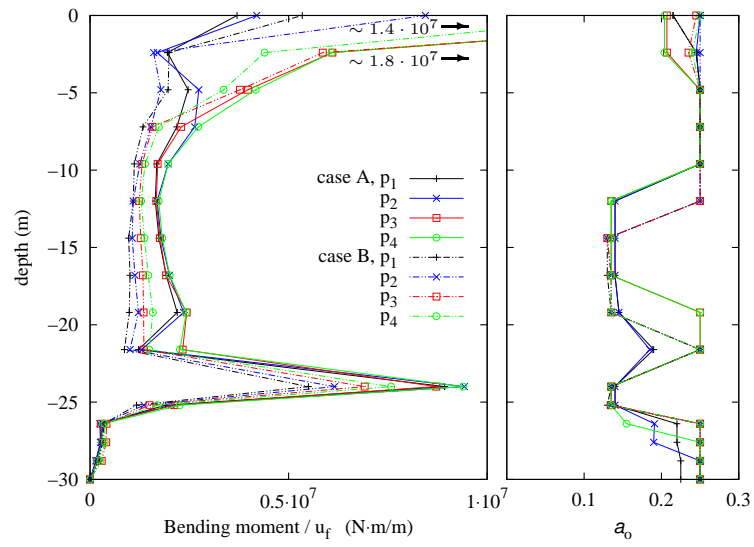


Figure 10: Comparison of envelopes of pile bending moments

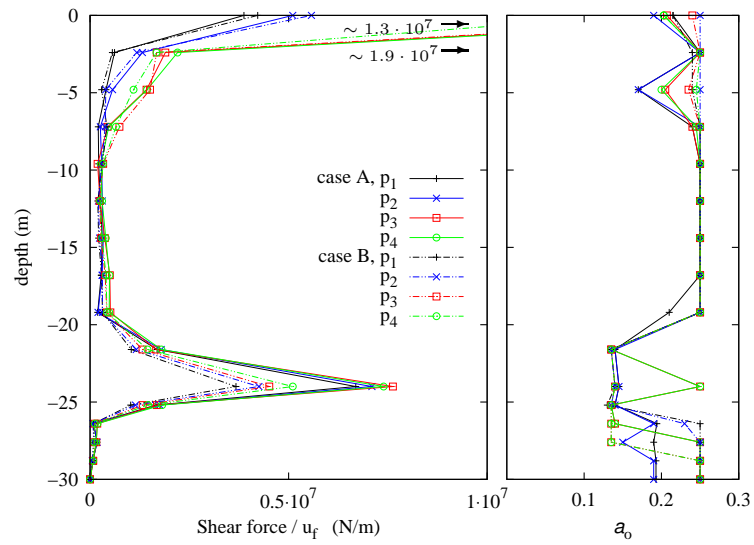


Figure 11: Comparison of envelopes of pile shear forces

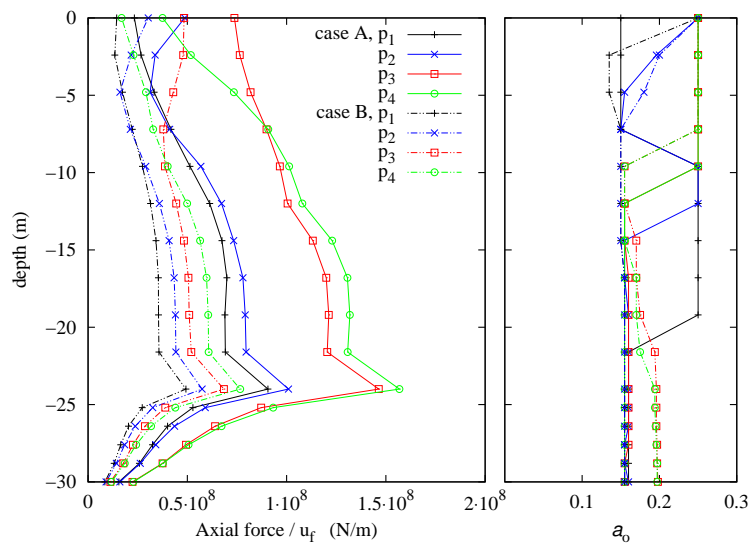


Figure 12: Comparison of envelopes of pile axial forces

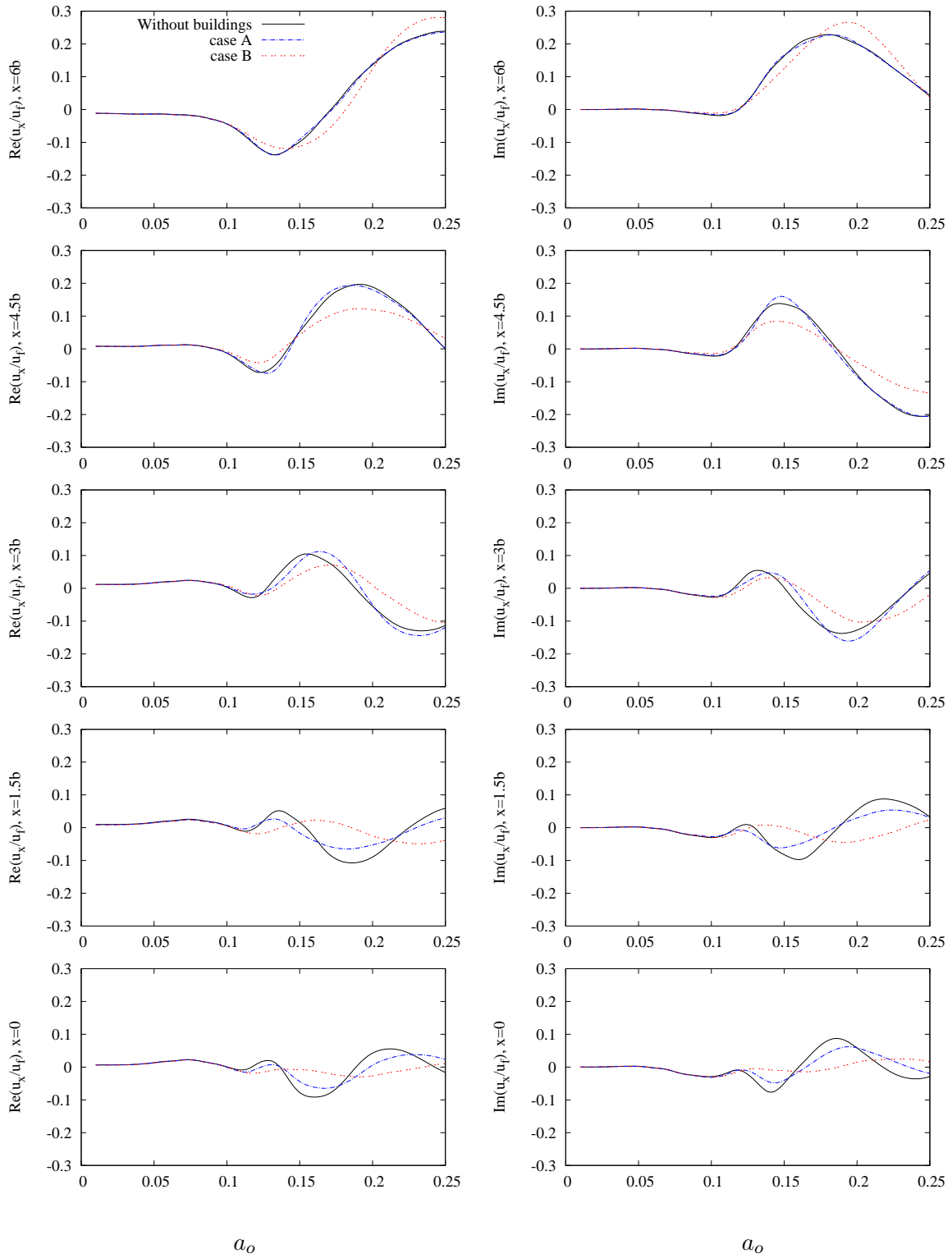


Figure 13: Comparison of horizontal displacements on different points in the ground surface.

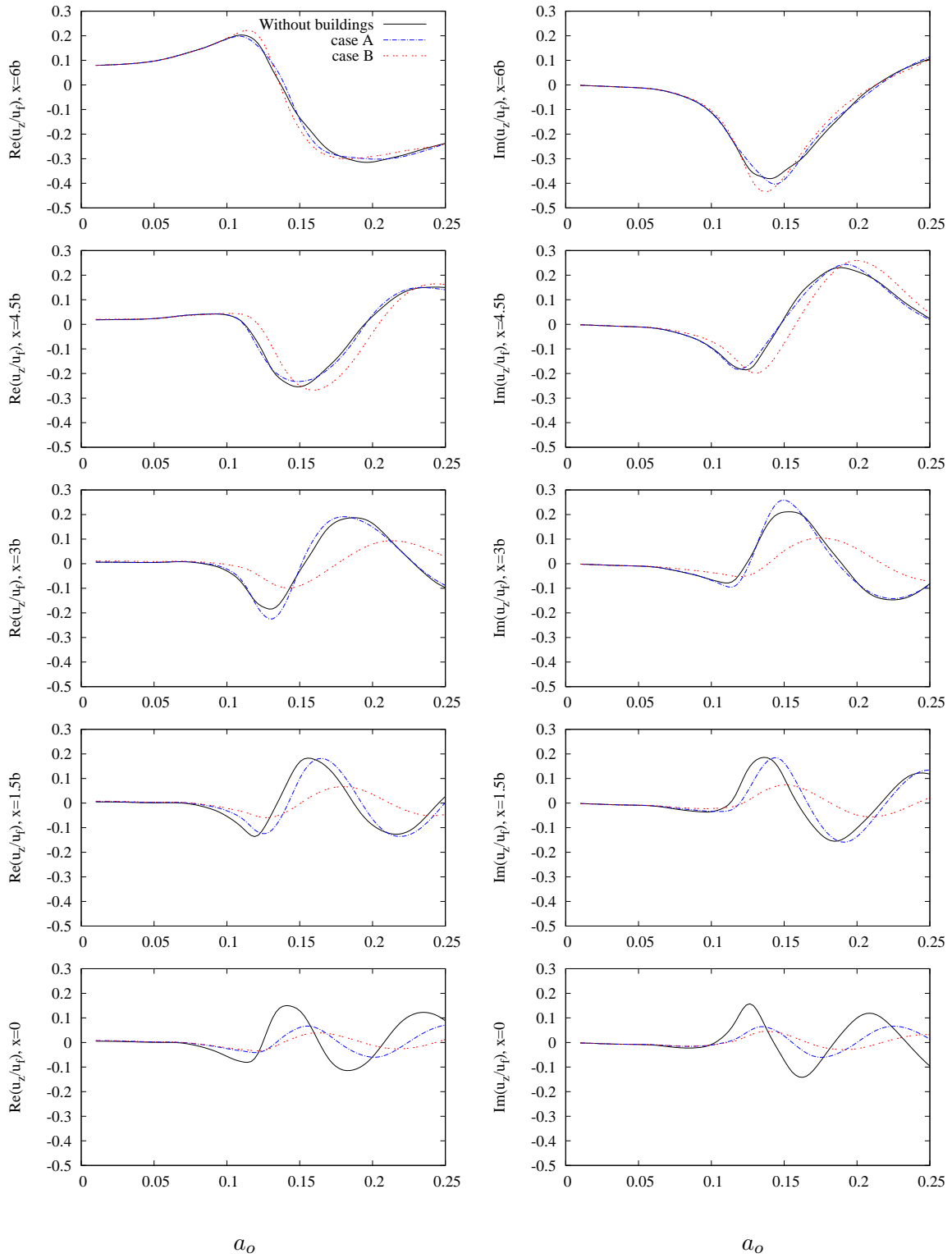


Figure 14: Comparison of vertical displacements on different points in the ground surface.

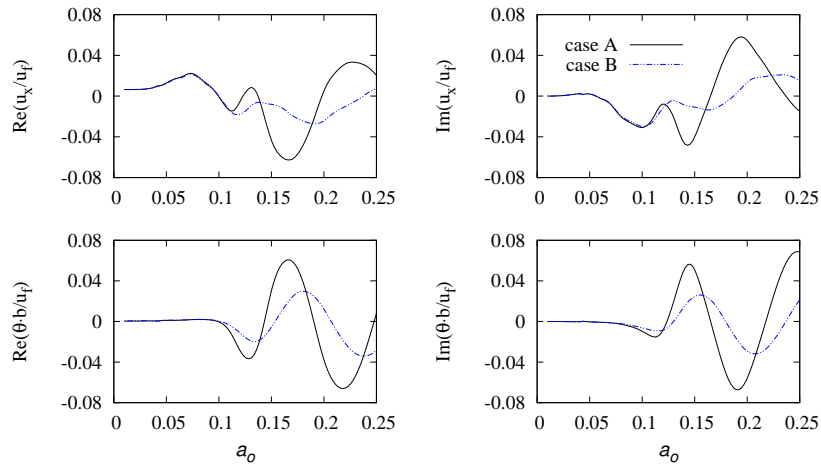


Figure 15: Horizontal displacements and rotations at pile cap of central building.

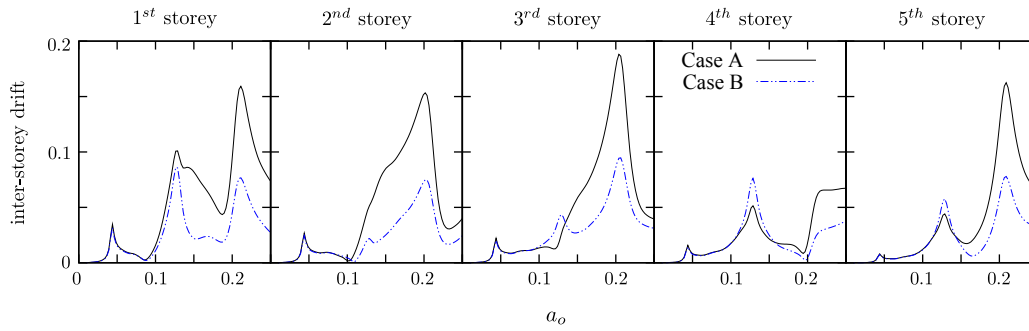


Figure 16: Inter-storey drift in each storey of central building.

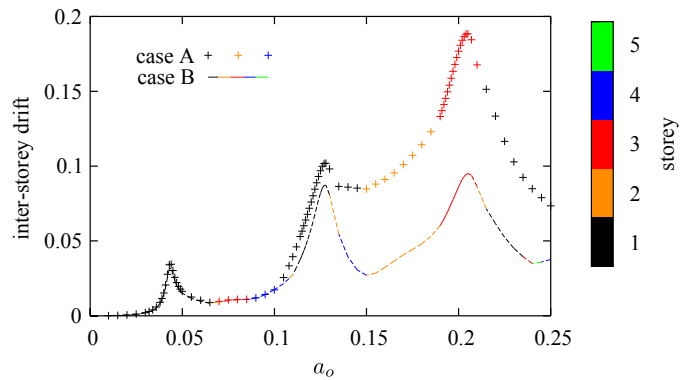


Figure 17: Maximum relative inter-storey drift in central building.